Evaluating microbial chemical choices: the ocean chemistry basis for the competition between use of O_2 or NO_3 as an electron acceptor

Peter G. Brewer[1], Andreas F. Hofmann[2], Edward T. Peltzer[1], William Ussler[1]

1. Monterey Bay Aquarium Research Institute (MBARI), 7700 Sandholdt Road, Moss Landing, CA 95039-9644, USA
2. German Aerospace Center (DLR), Institute of Technical Thermodynamics, Pfaffenwaldring 38–40, 70569 Stuttgart, Germany

Corresponding author:
Peter G. Brewer
brpe@mbari.org
Ph +1 -831-775-1706
Fax +1-831-775-1620

Abstract

The traditional ocean chemical explanation for the emergence of suboxia is that once O_2 levels decline to about 10 micromoles/kg then onset of NO_3 reduction occurs. This piece of ocean chemical lore is well founded in observations and is typically phrased as a microbial choice and not as an obligate requirement. The argument based on O_2 levels alone could also be phrased as being dependent on an equivalent amount of NO_3 that would yield the same energy gain. This description is based on the availability of the electron acceptor: but the oxidation reactions are usually written out as free energy yield per mole of organic matter, thus not addressing the oxidant availability constraint invoked by ocean scientists. Here we show that the argument can be phrased simply as competing rate processes dependent on the free energy yield ratio per amount of electron acceptor obtained, and thus the $[NO_3]$:$[O_2]$ ratio is the critical variable. The rate at which a microbe can acquire either O_2 or NO_3 to carry out the oxidation reactions is dependent on both the concentration in the bulk ocean, and on the diffusivity within the microbial external molecular boundary layer. From the free energy yield calculations combined with the ~25% greater diffusivity of the O_2 molecule we find that the equivalent energy yield occurs at a ratio of about 3.8 NO_3:O_2 for a typical Redfield ratio reaction, consistent with an ocean where NO_3 reduction onset occurs at about 10 μmol O_2: 40 μmol NO_3, and the reactions then proceed in parallel along a line of this slope until the next energy barrier is approached. Within highly localized microbial consortia intensely reducing pockets may occur in a bulk ocean containing finite low O_2 levels; and the local flux of reduced species from strongly reducing shelf sediments will perturb the large scale water column relationship. But all localized reactions drive towards maximal energy gain from their immediate diffusive surroundings, thus the ocean macroscopic chemical fields quite well approximate the net efficiency and operational mode of the ensemble microbial engine.

1 Introduction

One of the most prominent and widely recognized features of ocean biogeochemistry is the remarkable transition that occurs when dissolved oxygen levels become so low that microbes begin to utilize alternate electron acceptors and reduction of nitrate and the oxidised form of some other chemical species such as iodate can readily be observed (Rue et al., 1997). Biogeochemical profiles within intense oxygen minima clearly reveals the occurrence of a secondary nitrite peak, and a concomitant decline in nitrate concentration at these depths that is recognizable over huge areas of the ocean (Gruber, 2008; Ulloa et al., 2012; Thamdrup et al., 2012). Descriptions of this phenomenon occur in almost every ocean chemistry and biology text and the wording has become routine and near universally accepted. It is typically phrased approximately as "when O_2 levels decline below a critical level of about 10 μmol kg $^{-1}$ microbes turn to alternate electron acceptors ..." But this description appears to imply a choice, not an obligate condition, and thus could also be phrased as "when NO_3 levels become sufficiently high that the energy benefits of NO_3 reduction are equal to those available from reduction of O_2 then ..." The purpose of this paper is to provide a first step in clarifying the energy benefits of these ratios and relationships.

The first question a chemist might ask is "Why is the critical O_2 value set at 10?" – why not 20, or 5, or any other value? The second question might be to ask why the NO_3 value apparently becomes critical at that same point? And does temperature matter? – it usually does, but the apparent lack of a temperature dependence is typically not discussed and with the modern emergence of ocean warming and increasing deoxygenation some improved understanding of the fundamental controls of this apparent set point becomes important.

The standard phrasing in terms of only a lower limit for O_2 availability tacitly assumes that the well known Redfield C:N:O:P ratio holds, and that by specifying the dissolved O_2 concentration we are automatically specifying the equivalent NO_3 concentration. In practice this is only an approximation and changes in temperature and pressure which affect pO_2, and changes in NO_3 from e.g. local sources such as from agricultural run off or efflux from highly reducing sediments can effectively change these limits. One of the earliest and widely cited descriptions is that by Redfield et al. (1963) who drew upon waste water treatment literature. This classic chapter helped to define the field of marine biogeochemistry. Here it was stated as: "The order and extent to which these steps proceed depends on the free energy available from the respective reactions and on the concentration of the reactants. The free energy decreases in the order oxygen>nitrate>sulfate>carbonate when these serve as electron acceptors. ... With the exhaustion of oxygen, the oxidation of organic matter should continue by the reduction of nitrate." The phrase "exhaustion of oxygen" is of course not meant to be absolute but is typically set at some limiting value.

The original description by Redfield et al. (1963), and expanded upon by Richards (1965), is based on an assumed highly oxidizing initial external boundary condition, and the thermodynamic cascade described follows from this. This is applicable over vast volumes of ocean waters, and it is the process addressed here. But in some areas such as in the eastern tropical Pacific an additional boundary condition is provided by the efflux of chemical species (H_2S, CH_4, NH_3) from the highly reducing sediments and these will provide additional pathways for O_2 consumption.

Here we investigate the chemical driving forces behind these transformations by estimating both the free energy yield per mole of electron acceptor (O_2 versus NO_3) and also the diffusive boundary layer limitations that control the rate at which these species may be transported through the boundary layer surrounding microbial cells to derive various "crossover" concentrations and ratios. By this we mean the point at which a given nitrate consuming respiration process yields the same amount of energy per unit of time as does a given oxygen consuming process, thus making microbial nitrate consumption thermodynamically competitive with oxygen consumption.

2 Thermodynamic basis for quantifying energy yield and the diffusive electron acceptor supply rate

2.1 Standard free energy yield per mole of electron acceptor

Traditionally respiration reactions are tabulated according to their free energy yield per mole of available organic matter (e.g. Redfield et. al, 1963; Richards, 1965; Froelich et. al, 1979; Canfield et. al, 2005; Strohm et. al, 2007). But the ocean science description typically considers the sequence as occurring not on the basis of the availability of organic matter but on that of the electron acceptors thus requiring a re-writing of the standard form of the thermodynamic equations to match this.

The rate of supply of electron acceptors is typically not considered to be limiting yet as noted above this appears to be implied in the wording of the standard oceanographic descriptions. For example it is stated (Canfield et al., 2005) that the next following reaction (in terms of thermodynamic efficiency of organic matter use) commences once the "other electron acceptors are depleted". Froelich et al. (1979) report that: "When this oxidant is depleted, oxidation will proceed utilizing the next efficient ... oxidant". In this view an electron acceptor is either present in such an abundance so as not to pose any supply limitations on the efficiency of organic matter oxidation, or it is "depleted". This may mean either not present at all, or present in concentrations so low that supply limitations are present. It is also implied in these abbreviated descriptions that all organic matter oxidation is abruptly shifted to the next electron acceptor, whereas in practice a gradual transition may occur.

In practice observations show that once a critical threshold is reached oxygen levels continue to decline simultaneously with losses of NO_3; that is that oxic mineralisation and denitrification occur concurrently. Here we examine the energetics of this process as a continuum, a gradual shift with the utilization of multiple electron acceptor strategies as microbes seek to extract the maximum energy from their local environment. For this we need to calculate the supply limitations for the different electron acceptors.

The essential step required is to tabulate organic matter oxidation reactions in terms of their energy yield *per mole of electron acceptor*. We first show in Table 1 the standard representation of a tabulation of representative O_2 and NO_3^- consuming organic matter oxidation reactions (see Table A.1 in the appendix for an explicit redox-balance and references for these reactions) with their free energy yield values per Redfield ratio molecule ($\Delta G^{0,OM}$). We also list the more familiar per mole glucose equivalent ($\Delta G^{0,GL}$) as a comparative check. These values are derived from the standard energies of formation of the reactants and products (see Table A.2 in the appendix for an excerpt of Table 15 in Thauer et. al. (1977), which contains the relevant energies of formation).

In Table 2 we provide a re-formulated list of organic matter oxidation reactions with their free energy yields per mole of electron acceptor as required for matching to ocean observations of the profiles of O_2 and NO_3. In Table A.3 we provide further details on the exact steps required for reformulation of these equations. From these results it becomes clear as to which electron acceptor allows for the most efficient use of organic matter, or organic matter equivalents, and under which conditions.

2.2 Free energy yield ratio per amount of electron acceptor reacted

We first calculate an energy yield ratio (YR) per amount of electron acceptor for the various reaction pairs using the free energy yield values per mole of electron acceptor for the reactions given in Table 2

$$YR^{R_i^{O_2},R_j^{NO_3^-}} = \frac{\Delta G_{R_i}^{0,O_2}}{\Delta G_{R_j}^{0,NO_3^-}} \quad (1)$$

where the indices *i* and *j* indicate the pairing of reactions given in Table 2.

The upper panel of Table 3 shows $YR^{R_i^{O_2},R_j^{NO_3^-}}$ ratios per amount of electron acceptor reacted for all combinations of the oxygen and nitrate consuming reactions listed in Table 2.

From these yield ratios we then calculate an equivalence oxygen [O_2] concentration for a given nitrate concentration [NO_3] and a given reaction pair $R_i^{O_2}, R_j^{NO_3^-}$ such that the concentration ratio [NO_3^-]/[O_2] is equal to the energy yield ratio $YR^{R_i^{O_2},R_j^{NO_3^-}}$

$$[O_2]_{yr}^{R_i^{O_2},R_j^{NO_3^-}} = \frac{[NO_3^-]}{YR^{R_i^{O_2},R_j^{NO_3^-}}} \quad (2)$$

The lower panel of Table 3 shows equivalence oxygen concentration $[O_2]_{yr}^{R_i^{O_2},R_j^{NO_3^-}}$ values for a given NO_3 concentration for each combination of the reactions shown in Table 2.

2.3 Maximal electron acceptor diffusion limited energy yield of a respiration reaction

Electron acceptors need to be transported to the cell across the diffusive boundary layer (DBL). This diffusive electron acceptor supply can be the ultimately limiting criterion for microorganism growth and survival and has been shown to be critical even at very low levels (Stolper et al., 2010). Diffusive electron acceptor EA (either O_2 or NO_3^- here) flux per area of exchange across the DBL around a respiring microorganism can be expressed by the standard discretization of Fick's first law (eg., Santschi et al., 1991; Boudreau,1996; Zeebe, 2001; Hofmann et. al., 2011b,a).

$$F_D^{EA} = \frac{D^{EA}}{L} \left([EA]_f - [EA]_s\right) \quad (3)$$

With F_D being the diffusive flux of electron acceptor EA in μmol s^{-1} cm^{-2} across the DBL, D^{EA} the molecular diffusion coefficient for the electron acceptor EA in cm^2 s^{-1}, $[EA]_f$ and $[EA]_s$ the electron acceptor EA concentrations in the free stream (subscript f) and at the surface of the organism (subscript s) in μmol cm^{-3}. L is the thickness of the diffusive boundary layer in cm. All diffusivities used are taken at a standard temperature of 5°C and in sea water.

For particles much smaller than the smallest eddies (diameter of ≈1 mm), the effective thickness of the DBL is set by the radius of the spherical organism (Zeebe and Wolf-Gladrow, 2001, p. 133 & 135). We thus assume L = r with r = 0.5 10^{-4} being the assumed standard radius of a spherical microorganism (about the size of the denitrifying bacterium (Canfield et. al., 2005)). With A = $4\pi r^2$ being the surface area of the microorganism, this yields an expression for the total diffusive electron acceptor flux per organism in μmol s^{-1} of

$$F_D^{EA} = 4\ \pi\ r\ D^{EA} \left([EA]_f - [EA]_s\right) \quad (4)$$

Equation 4 is an expression commonly used to describe limitations of diffusive boundary layer transport around microorganisms (e.g. Stolper et. al., 2010) and can be modified to represent electron acceptor concentrations $[EA]_f$ and $[EA]_s$ in gravimetric units of μmol kg^{-1} with ρ_{SW}, the density of seawater in kg cm^{-3}.

$$F_D^{EA} = 4\ \pi\ r\ D^{EA}\ \rho_{SW} \left([EA]_f - [EA]_s\right) \quad (5)$$

Because our objective is to describe the oceanic supply side limited by physico-chemical processes in the ocean in a non-organism specific way, we assume $[EA]_s = 0 \mu molkg^{-1}$, i.e assuming maximally efficient electron acceptor transport into the cell. The expression for the diffusive electron acceptor flux can thus be simplified to

$$F_D^{EA} = 4\ \pi\ r\ D^{EA}\ \rho_{SW}\ [EA]_f \quad (6)$$

Assuming diffusion limitation for the electron acceptor [EA] flux to the cell, a maximal energy yield rate in nJ s^{-1} for a given respiration reaction R_i^{EA} can then be calculated.

$$E_{max}^{R_i^{EA}} = F_D^{EA} \quad \Delta G_{R_i^{EA}}^{0,EA} \quad (7)$$

2.4 Electron acceptor concentration crossover point for equal electron-acceptor-diffusion-limited energy yield

Based on $E_{max}^{R_i^{EA}}$ values, one can calculate concentrations [O_2] and [NO_3^-], for two given

respiration reactions $R_i^{O_2}$ and $R_j^{NO_3^-}$ where $E_{max}^{R_i^{O_2}} = E_{max}^{R_j^{NO_3^-}}$, meaning both reactions, when running at their electron-acceptor-diffusion-limited rate, yield the same amount of energy per unit of time.

For a given nitrate concentration $[NO_3^-]$, the corresponding oxygen concentration $[O_2]_{cr}^{R_i^{O_2},R_j^{NO_3^-}}$ at the "energy crossover point" can be defined as

$$[O_2]_{cr}^{R_i^{O_2},R_j^{NO_3^-}} := E_{max}^{R_i^{O_2}}\left([O_2]_{cr}^{i,j}\right) \stackrel{!}{=} E_{max}^{R_j^{NO_3^-}}\left([NO_3^-]\right) \quad (8)$$

Figure 1 provides a detailed graphical explanation of the definition of $[O_2]_{cr}^{R_i^{O_2},R_j^{NO_3^-}}$. The nitrate – oxygen crossover ratio $CR^{R_i^{O_2},R_j^{NO_3^-}}$ at the point of equal electron-acceptor-diffusion-limited energy yield for the two paired reactions can then be calculated as

$$CR^{R_i^{O_2},R_j^{NO_3^-}} = \frac{[NO_3^-]}{[O_2]_{cr}^{i,j}} \quad (9)$$

Table 3 shows $[O_2]_{cr}^{R_i^{O_2},R_j^{NO_3^-}}$ (upper panel) and $CR^{R_i^{O_2},R_j^{NO_3^-}}$ (lower panel) for all combinations of each an oxygen and a nitrate consuming reaction from Table 2.

3 Discussion

The physico-chemical descriptions given here are intended to be reasonable approximations to the opportunities presented to microbes as they seek to extract the maximum chemical energy from their environment. The arguments cannot be true in the instantaneous sense as intense local gradients come and go, but these should be a good match over longer space and time scales. We assume that microbes are near perfect chemical engineers and can be quickly out-competed if a more favorable energetic pathway emerges within their detection space.

3.1 Model Assumptions

For simplicity we have used only the standard free energies (ΔG^0). This requires that we assume the respiratory quotient Q in the equation

$$\Delta G = \Delta G^0 + RT\ln(Q) \quad (10)$$

to be equal to 1. This naturally follows from our objective of describing the "oceanic supply side", i.e. the boundary layer limitations outside of the organism only, as then [EA], the concentration of the electron acceptor (either O_2 or NO_3^-) inside the cell - i.e. the variable quantity that might effect Q in our calculations - is not clearly defined. This appears to be reasonable again if very short term changes in Q are neglected since this implies maximum utilization of the resource on the larger scale.

We therefore assume that inside the microbe there are mechanisms bringing the concentration ratio Q always to a certain favored value. This will happen at required energy spent, but we assume that there is always enough energy (organic matter + oxidising agent) available. Thus for our calculations and relative comparisons we assume (without loss of generality), that Q = 1 always, which renders the term $RT\ln(Q)$ zero. This allows us to use ΔG^0 values for all our calculations.

As a consequence, the absolute energy gains $E_{max}^{R_i^{EA}}$ per unit of time that we calculate (cf. Fig. 1) are not the exact energy values found in nature, but are maximal values used for relative intercomparison of different organic matter reactions. Since a focus of our work is to assess the chemical ratios in the bulk ocean at which this transition occurs then absolute values are not necessary and this relative comparison is sound. As noted above the calculated $CR^{R_i^{O_2},R_j^{NO_3^-}}$ values only consider standard free energy and external diffusive limitation considerations for the primary oxidants O_2 and NO_3^-; other trace chemical species are present and the reduction of IO_3^- readily occurs, but these concentrations are so low that they do not affect the larger scale properties. As a first approximation we use concentrations, not partial pressures (for O_2) and activities (for NO_3^-) to avoid unneccessary complicated considerations. These may readily be included in later studies of cross-over ratios if required. An example of the formal inclusion of the partial pressure terms within diffusive boundary layer fluxes is given in Hofmann et al. (2013a).

For all our calculations we use a constant temperature of 5°C . There is only a small change in the temperature dependence of the concentration crossover ratio $CR^{R_i^{O_2},R_j^{NO_3^-}}$ since the diffusion coefficients for O_2 and NO_3^- have only slightly different slopes with temperature (Fig. 2). This may be significant when comparing ratios for warm surface waters and cold deep waters (similar to the arguments concerning hypoxia given in Hofmann et. al., 2011c) and against the backdrop of global oceanic warming (Lyman et. al., 2010).

We show in Fig. 2 the temperature dependency of diffusive boundary layer transport limitation of electron acceptor supply only; it may be possible that other processes, especially inside the microbial cell might exhibit a much stronger temperature dependency but we not aware of any evidence for this. Also, if O_2 and NO_3^- reactions in the cell happen at different respiratory quotients Q (i.e., not Q=1 as assumed here), then the there may be a differential temperature effect on the free energy yield of the O_2 reaction vs. the NO_3^- reaction; again, we expect any such effect to be small.

We are aware that assuming the electron acceptor concentration directly at the surface of the organism to be zero, i.e. $[EA]_s = 0 \mu molkg^{-1}$, assumes a high rate of electron acceptor transport into the cell. Other authors assume, e.g. $[EA]_s = 0.5\ [EA]_f$ (Stolper et. al., 2010). Here we are concerned mainly with relative energy comparisons between various reactions and wanted to provide an outer envelope for the oceanic ”supply side“ that each organism faces. For those reasons and to obtain more tractable mathematical expressions, we choose to assume $[EA]_s = 0 \mu molkg^{-1}$. As a result, obtained $E_{max}^{R_i^{EA}}$ values may overestimate true values, however the energy crossover ratios and concentrations that are the focus here are not affected by this assumption.

3.2 Free energy only vs. diffusion limitation and free energy

As a comparison between Tables 3 and 4 shows, the pure energy yield ratios $YR^{R_i^{O_2},R_j^{NO_3^-}}$ are considerably smaller than $CR^{R_i^{O_2},R_j^{NO_3^-}}$ ratios which additionally include diffusive limitations for both electron acceptors. This is a direct effect of the higher diffusivity of oxygen as compared to nitrate and it shows that looking at only the free energies would underestimate the difference in thermodynamic efficiency between O_2 and NO_3^- reactions; importantly considering the diffusive limitation changes the energy yield ratio between oxygen consuming and nitrate consuming reactions by about 25 % and this appears to be key in matching observations to theory.

3.3 Crossover points derived here vs. classical thresholds and in situ data

Fig. 3 shows the $[NO_3^-]$ vs. $[O_2]$ free energy and diffusive limitation crossover lines ($[O_2]_{cr}^{R_i^{O_2},R_j^{NO_3^-}}([NO_3^-])$) for three different reaction combinations: oxic mineralisation ($R_1^{O_2}$) and denitrification to NO_2^- ($R_7^{NO_3^-}$): blue line; oxic mineralisation and denitrification to NO_2^- including the oxidation of the organic matter amines ($R_8^{NO_3^-}$): red line; as well as oxic mineralisation including the oxidation of the organic matter amines ($R_2^{O_2}$) and denitrification to NO_2^-: black line. Dashed horizontal and vertical lines represent typical nitrate concentrations and typical oxygen concentration thresholds for the onset of suboxia.

The crossover points of the horizontal and vertical lines fall close to all energy and diffusive limitation crossover lines, which makes our theoretical calculations consistent to classical observed ocean thresholds. The crossover point between the suboxia threshold $[O_2] = 10\ \mu$ mol kg^{-1} amd the nitrate concentration around the oxygen minimum zone and the onset of nitrate consumption in the open Pacific $[NO_3^-] = 30\ \mu$ mol kg^{-1} is very close to the black $CR^{R_2^{O_2},R_7^{NO_3^-}}$ crossover line, which might be interpreted as a strong hint towards the dominant reactions occurring in the open ocean. Similarly, the crossover point between $[O_2] = 10\ \mu$ mol kg^{-1} and $[NO_3^-] = 40\ \mu$ mol kg^{-1}, the nitrate concentration at the inflection point of the nitrate profile in Santa Monica Bay is close to the red and blue $CR^{R_1^{O_2},R_7^{NO_3^-}}$ and $CR^{R_1^{O_2},R_8^{NO_3^-}}$ crossover lines and might be similarly interpreted as dominant in that local environment.

Figure 4 shows depth profiles of $[O_2]$, $[NO_3^-]$, $[O_2]_{cr}^{R_1^{O_2},R_7^{NO_3^-}}$ (oxic mineralisation vs. denitrification to NO_2^-), and $[O_2]_{cr}^{R_1^{O_2},R_8^{NO_3^-}}$ (oxic mineralisation vs. denitrification to NO_2^- incl. oxidation of the organic matter amines) in Santa Monica Basin. These data were obtained by us in an AUV survey carried out in June 2011 (Hofmann et al., 2013c). It can be seen that $[O_2]_{cr}^{R_1^{O_2},R_7^{NO_3^-}}$ intersects $[O_2]$ at about 650 m depth (Fig. 4, left panel), the same depth as the inflection of the nitrate concentration profile (Fig. 4, right panel). Similar nitrate drawdowns in a mid-water oxygen minimum zone in the Pacific are argued to be the result of water column denitrification (e.g. Rue et. al.,1997), while for Santa Monica Basin and other Southern California basins, it is argued that all denitrification happens in the sediments and draws down water column

nitrate concentrations (Berelson et.al.,1987, 1996). Sigman et. al., (2003) estimate, based upon the NO_3 N_{15}/N_{14} isotope ratio, that 75% of the observed decrease in the Santa Barbara basin is due to sedimentary denitrification.

Our calculations show that the inflection in the nitrate profile, both locally around the southern California Basins and far more broadly within the intense OMZ of the eastern tropical Pacific, happens at the same depth at where oxic mineralisation and denitrification to NO_2^- become equally thermodynamically efficient when their standard free energies and diffusive electron acceptor supply limitations are considered. The thermodynamic basis is the same for these scenarios, but the local intensity drives our perception of the dominant signal source.

4 Conclusions & Outlook

We believe that these relationships offer an improved description of the conditions for the onset of suboxia and the sucession of organic matter oxidation reactions with various electron acceptors. The classical wording implying that the succession of organic matter oxidation reactions is a series of "step-functions" has been known to be outmoded for some time but improved descriptions of the energetic basis for this have only been latently acknowledged and we have not been able to find a specific account. Clearly O_2 consumers do not stop consuming O_2 when NO_3^- reduction becomes favorable and the reactions appear in parallel. Thus a continuum or a gradual succession process, where the transition can be tied to the 50:50 energy efficiency crossover points between organic matter oxidation with different electron acceptors, appears to be better able to describe ocean processes. For the onset of suboxia, it is clear that a certain $\frac{[NO_3^-]}{[O_2]}$ ratio has to be the key. These arguments can only go so far and it appears that the next major transition, that of SO_4 reduction, is controlled by the functional absolute loss of O_2 and not by a ratio. We have not considered here several other possibilities involving metal ions such as Mn and Fe based reactions.

When looking at the electron acceptor sucession as a continuous process governed by electron acceptor supply, it is required that an electron acceptor is not only assumed to be present "sufficiently" or to be "depleted", but that physico-chemical supply limitations of the electron acceptors have to be made explicit. Calculations based solely on the chemical free energy terms do not yield a result that usefully mimics the observed ocean. But by including the diffusive terms and accounting for the ~ 25% increased diffusivity of the O_2 molecule over the NO_3 ion then a much better fit is found. The apparent lack of a temperature dependence appears simply to be due to the fact that all reactants are contained within the Redfield ratio in constant proportions, and that the temperature dependence of the diffusivity of O_2 and NO_3 is very similar. We note that these relationships may be experimentally testable.

We only describe processes happening outside the microbial cell - i.e. we describe the "oceanic supply side". True measured nitrate to oxygen crossover ratios may be organism specific depending on exact local micro-environments and reaction pathways that are favored. Field data and laboratory experiments can surely shed more light on this matter, both in terms of a census of microorganisms in certain environments, but also in terms of net ecosystem function such as in estimates of the large scale estuarine filter function (Hofmann et al., 2008) under varying nitrate vs. oxygen ratios.

Determining criteria that can predict the onset of suboxia and nitrate consumption is

especially important since declining oceanic oxygen concentrations due to climate change (e.g. Nakanowatari et. al., 2007; Stramma et. al., 2008; Helm et al., 2011) will bring many low oxygen systems close to the $\frac{[NO_3^-]}{[O_2]}$ "crossover point" where NO_3^- will begin to be consumed.

From our calculations it is clear that the oxidative capacity of the oceanic NO_3 system is quite small, and for a typical maximum concentration of about 40 μmol/kg the equivalent O_2 concentration is only about 12 μmol. Since the loss of O_2 from the solubility effect alone of an ocean warming of 2° is about 14 μmol then even this modest effect will exceed the NO_3 capacity as a buffer against emergent anoxia. In practice the solubility term appears to explain only 15% of the O_2 losses now being observed (Helm et al., 2011) and it appears inevitable that given the functional anoxia that now exists in some areas (Canfield et al., 2010) will transfom into a true anoxic zone with the permament emergence of free sulfide in the ocean water column. There is no record of this in modern times although sporadic sulfide eruptions have been observed (Weeks et. al., 2004) and thus it would seem to be a true and deeply disturbing "tipping point" for the ocean with the NO_3 buffer offering only very modest protection.

We also note that there are many other processes involving nitrogen transformations and the analysis provided here considers only one, although major, facet of the reaction complex. For example we do not here consider the possible pH dependencies although the transition from microbial production of NO_3 to microbial utilization of NO_3 involves the switch from acidic export to acidic import.

Acknowledgements

This work was supported by a grant to the Monterey Bay Aquarium Research Institute from the David & Lucile Packard Foundation.

References

Berelson, W. M., Hammond, D. E., Johnson, K. S., 1987. Benthic fluxes and the cycling of biogenic silica and carbon in two southern california USA borderland basins. Geochim. Cosmochim. Acta 51,1345–1364.

Berelson, W. M., McManus, J., Coale, K. H., Johnson, K. S., Kilgore, T., Burdige, D., Pilskaln, C., 1996. Biogenic matter diagenesis on the sea floor: A comparison between two continental margin transects. J. Mar. Res. 54, 731–762.

Boudreau, B. P. 1996. Diagenetic Models and Their Implementation, Springer, Berlin, pp. 13823-13846.

Canfield, D., Thamdrup, B., Kristensen, E., 2005. Aquatic Geomicrobiology. Elsevier Academic Press, Advances in Marine Biology, Volume 48.

Canfield, D.E., Stewart, F.J., Thamdrup, B., De Brabandere, L., Dalsgaard, T., DeLong, E.F., Revsbech, N.P., and Ulloa, O. 2010. A cryptic sulfur cycle in the oxygen-minimum-zone waters off the Chilean Coast. Science, 330, 1375-1378.

Froelich, P. N., Klinkhammer, G. P., Bender, M. L., Luedtke, N. A., Heath, G. R., Cullen, D., Dauphin, P., Hammond, D., Hartman, B., Maynard, V., 1979. Early Oxidation of Organic-Matter

in Pelagic Sediments of the Eastern Equatorial Atlantic - Suboxic Diagenesis. Geochim. Cosmochim. Acta 43, 1075–1090.

Gruber, N. 2008. The marine nitrogen cycle: Overview and Challenges, in *Nitrogen in the Marine Environment* (eds: Capone, D. G., Bronk, D. A., Mulholland, M. R. & Carpenter, E. J.) Elsevier, pp. 1–50.

Helm, K. P., Bindoff, N. L., and Church, J. A. 2011. Observed decreases in oxygen content of the global ocean, Geophys. Res. Lett., 38, L23 602.

Hofmann, A. F., Soetaert, K., Middelburg, J. J., 2008. Present nitrogen and carbon dynamics in the Scheldt estuary using a novel 1-D model. Biogeosciences 5, 981–1006.

Hofmann, A. F., Peltzer, E. T., Walz, P., Brewer, P. G., 2011. Hypoxia by degrees: Establishing definitions for a changing ocean. Deep-Sea Res. Part I 58, 1212–1226.

Hofmann, A.F., Peltzer, E.T., and Brewer, P.G. (2013a) Kinetic bottlenecks to chemical exchange rates for deep-sea animals I: Oxygen. Biogeosciences, 9, 13817-13856, doi:10.5194/bgd-9-13817-2012 .

Hofmann. A.F., Peltzer, E.T., and Brewer, P.G. (2013b) Kinetic bottlenecks to chemical exchange rates for deep-sea animals II: Carbon Dioxide. Biogeosciences, 9, 15787-15821,doi:10.5194/bgd-9-15787-2012.

Hofmann, A.F., P.M. Walz, H. Thomas, E.T. Peltzer and P.G. Brewer (2013c) High resolution topography-following mapping of ocean hypoxia using an autonomous underwater vehicle: the limits of the Santa Monica Basin “dead zone.” J. Atmos. Ocean. Technol., doi: 10.1175/JTECH-D-12-00249.17-1582.

Lyman, J. M., Good, S. A., Gouretski, V. V., Ishii, M., Johnson, G. C., Palmer, M. D., Smith, D. M., Willis, J. K., 2010. Robust warming of the global upper ocean. Nature 465, 334–337.

Nakanowatari, T., Ohshima, K. I., Wakatsuchi, M., 2007. Warming and oxygen decrease of intermediate water in the northwestern north pacific, originating from the Sea of Okhotsk, 1955–2004. Geophys. Res. Lett. 34 (4),L04602.

Redfield, A. C., Ketchum, B. H., Richards, F. A., 1963. The influence of organisms on the composition of seawater, in *The Sea*. Vol. 2. Wiley, New York, Ch. 2, pp. 26–77.

Richards, F.A. 1965. Anoxic basins and fjords. In: Riley, J.P., Skirrow, G. (Eds.) Chemical Oceanography. Academic Press, London, pp. 611-643.

Rue, E., Smith, G., Cutter, G., Bruland, K.1997. The response of trace element redox couples to suboxic conditions in the water column. Deep-Sea Res. Part I 44, 113–134.

Santschi, P. H., Anderson, R. F., Fleisher, M. Q., Bowles, W., 1991.Measurements of diffusive sublayer thicknesses in the ocean by alabaster dissolution, and their implications for the measurements of benthic fluxes. J. Geophys. Res. 96 (C6), 10641–10657.

Sayama, M., Risgaard-Petersen, N., Nielsen, L. P., Fossing, H., Christensen, P. B., 2005. Impact of bacterial NO_3^- transport on sediment biogeochemistry. Appl. Environ. Microbiol. 71, 7575–7577.

Shaffer, G., Olsen, S. M., Pedersen, J. O. P. 2009. Long-term ocean oxygen depletion in response to carbon dioxide emissions from fossil fuels. Nature Geosciences 2, 105–109.

Sigman, D. M., Robinson, R., Knapp, A. N., van Geen, A., McCorkle, D. C., Brandes, J. A., Thunell, R. C., 2003. Distinguishing between water column and sedimentary denitrification in the Santa Barbara basin using the stable isotopes of nitrate. Geochem. Geophys. Sys., 1040, doi:10.1029/2002GC000384

Stolper, D. A., Revsbech, N. P., Canfield, D. E., 2010. Aerobic growth at nanomolar oxygen concentrations. Proc. Natl. Acad. Sci. U.S. 107, 18755–18760.

Stramma, L., Johnson, G. C., Sprintall, J., Mohrholz, V., 2008. Expanding oxygen-minimum zones in the tropical oceans. Science 320, 655–658.

Strohm, T. O., Griffin, B., Zumft, W. G., Schink, B., 2007. Growth yields in bacterial denitrification and nitrate ammonification. Appl. Environ. Microbiol. 73, 1420–1424.

Thamdrup, B., T. Dalsgaard, and R. N. P., 2012: Widespread functional anoxia in the oxygen minimum zone of the eastern south Pacific. Deep Sea Research I, 65, 36-45.

Thauer, R. K., Jungermann, K., Decker, K., 1977. Energy conservation in chemotropic anaerobic bacteria. Bacteriological Reviews 41 (1), 100–180.

Ulloa, O., Canfield, D., DeLong, E.F., Letelier, R.M., Stewart, F.J. 2012. Microbial oceanography of anoxic oxygen minimum zones. Proc. Natl. Acad. Sci., USA, 109, 15996-16003 doi:/10.1073/pnas.1205009109.

Weeks,S. J., Currie, B., Bakun, A., Peard, K. R. 2004. Hydrogen sulphide eruptions in the atlantic ocean off southern africa: implications of a new view based on seawifs satellite imagery. Deep Sea Res. Part I 51, 153-172.

Zeebe, R. E., Wolf-Gladrow, D., 2001. CO_2 in Seawater: Equilibrium, Kinetics, Isotopes, 1st Edition. No. 65 in Elsevier Oceanography Series. Elsevier. 2.3.

symbol	name	reaction	$\Delta G^{0,OM}$	$\Delta G^{0,GL}$
$R_2^{O_2}$	oxic min. incl. NH_3 ox.	$(CH_2O)_{106}(NH_3)_{16} + 138O_2 -> 106CO_2 + 16HNO_3 + 122H_2O$	-56528	-3200
$R_3^{NO_3^-}$	denitrification incl. NH_3 ox.	$(CH_2O)_{106}(NH_3)_{16} + 94.4HNO_3 -> 106CO_2 + 55.2N_2 + 177.2H_2O$	-52926	-3000
$R_1^{O_2}$	oxic mineralization	$(CH_2O)_{106}(NH3)_{16} + 106O_2 -> 106CO_2 + 16NH_3 + 106H_2O$	-50739	-2870
$R_2^{NO_3^-}$	denitrification to N_2	$(CH_2O)_{106}(NH_3)_{16} + 84.8HNO_3 -> 106CO_2 + 16NH_3 + 42.4N_2 + 148.4H_2O$	-47972	-2710
$R_8^{NO_3^-}$	denitrification to NO_2- incl. NH_3 ox.	$(CH_2O)_{106}(NH3)_{16} + 260HNO_3 -> 106CO_2 + 276HNO_2 + 122H_2O$	-36065	-2040
$R_7^{NO_3^-}$	denitrification to NO_2-	$(CH_2O)_{106}(NH_3)_{16} + 212HNO_3 -> 106CO_2 + 212HNO_2 + 16NH_3 + 106H_2O$	-35021	-1980
$R_1^{NO_3^-}$	ammonification	$(CH_2O)_{106}(NH_3)_{16} + 53HNO_3 -> 106CO_2 + 69NH_3 + 53H_2O$	-31562	-1790

Table 1: Representative organic matter oxidation reactions. Standard free energy gain values in $\frac{\text{kJ}}{\text{mol}}$ - per mole of organic matter with Redfield stoichiometry in C and N ($\Delta G^{0,OM}$) and per mole of glucose equivalent ($\Delta G^{0,GL}$), as derived from the energies of formation of the reactants and product given in Thauer et al.(1977). $R_1^{O_2}$ and $R_1^{NO_3^-}$: (e.g. Strohm et al., 2007); $R_2^{O_2}$, $R_2^{NO_3^-}$ and $R_8^{NO_3^-}$: (e.g. Froelich et al. 1979). See Table A.1 for explicit redox balances of all reactions. By dividing the value for oxic mineralisation by $\frac{106}{6} \approx 17.67$ (Froelich et al. 1979) to get to a value per mol of glucose, one obtains $\Delta G^{0\prime} \approx$ -2870 $\frac{\text{kJ}}{\text{mol}}$, consistent with Eq. 1 in Strohm et al. (2007).

symbol	name	reaction	$\Delta G^{0,EA}$
$R_1^{NO_3^-}$	ammonification	$HNO3 + \frac{1}{53}((CH2O)_{106}(NH3)_{16}) -> 2CO2 + \frac{69}{53}NH3 + H2O$	-596
$R_2^{NO_3^-}$	denitrification to N_2	$HNO3 + \frac{5}{424}((CH2O)_{106}(NH3)_{16}) -> \frac{5}{4}CO2 + \frac{10}{53}NH3 + \frac{1}{2}N2 + \frac{7}{4}H2O$	-566
$R_3^{NO_3^-}$	denitrification incl. NH_3 ox.	$HNO3 + \frac{5}{472}((CH2O)_{106}(NH3)_{16}) -> \frac{265}{236}CO2 + \frac{69}{118}N2 + \frac{443}{236}H2O$	-561
$R_1^{O_2}$	oxic mineralization	$O2 + \frac{1}{106}((CH2O)_{106}(NH3)_{16}) -> CO2 + \frac{16}{106}NH3 + H2O$	-479
$R_4^{NO_3^-}$	H_2S ox. w. NO_3- (1st step)	$NO3 - +4H2S + 2H + -> 4S^0 + NH4 + +3H2O$	-466
$R_5^{NO_3^-}$	H_2S ox. w. NO_3- (2nd step)	$NO3 - +\frac{7}{3}H2O + \frac{4}{3}S^0 -> NH4 + +\frac{4}{3}SO4^{2-} + \frac{2}{3}H +$	-434
$R_2^{O_2}$	oxic min. incl. NH_3 ox.	$O2 + \frac{1}{138}((CH2O)_{106}(NH3)_{16}) -> \frac{53}{69}CO2 + \frac{8}{69}HNO3 + \frac{61}{69}H2O$	-410
$R_6^{NO_3^-}$	H_2S ox. w. NO_3- (combined)	$NO3 - +H2S + H2O -> NH4 + +SO4^{2-}$	-326
$R_7^{NO_3^-}$	denitrification to NO_2-	$HNO3 + \frac{1}{212}(CH2O)_{106}(NH3)_{16} -> \frac{1}{2}CO2 + HNO2 + \frac{4}{53}NH3 + \frac{1}{2}H2O$	-165
$R_8^{NO_3^-}$	denitrification to NO_2- incl. NH_3 ox.	$HNO3 + \frac{1}{260}((CH2O)_{106}(NH3)_{16}) + -> \frac{53}{130}CO2 + \frac{69}{65}HNO2 + \frac{61}{130}H2O$	-139

Table 2: Representative organic matter oxidation reactions and dissimilatory nitrate reduction coupled to hydrogen sulfide oxidation (Sayama et al., 2005) tabulated according to their free energy yield per mole of electron (e^-) acceptor ($\Delta G^{0,EA}$) $\Delta G^{0,EA}$ values are in $\frac{\text{kJ}}{\text{mol}}$ - per mole of electron (e^-) acceptor, as derived from the energies of formation of the reactants and product given in Thauer et al. (1977). Reaction equations from Table 1 are reformulated as detailed in table 7.

$\mathbf{YR}^{\mathbf{R_i^{O_2}},\mathbf{R_j^{NO_3^-}}}$	$R_1^{NO_3^-}$	$R_2^{NO_3^-}$	$R_3^{NO_3^-}$	$R_4^{NO_3^-}$	$R_5^{NO_3^-}$	$R_6^{NO_3^-}$	$R_7^{NO_3^-}$	$R_8^{NO_3^-}$
$R_1^{O_2}$	0.80	0.85	0.85	1.03	1.10	1.47	2.90	3.45
$R_2^{O_2}$	0.69	0.72	0.73	0.88	0.94	1.26	2.48	2.95

$[\mathbf{O_2}]_{\mathbf{yr}}^{\mathbf{R_i^{O_2}},\mathbf{R_j^{NO_3^-}}}$	$R_1^{NO_3^-}$	$R_2^{NO_3^-}$	$R_3^{NO_3^-}$	$R_4^{NO_3^-}$	$R_5^{NO_3^-}$	$R_6^{NO_3^-}$	$R_7^{NO_3^-}$	$R_8^{NO_3^-}$
$R_1^{O_2}$	49.8	47.3	46.8	38.9	36.2	27.2	13.8	11.6
$R_2^{O_2}$	58.1	55.2	54.7	45.5	42.3	31.8	16.1	13.6

Table 3: Free energy yield ratio $YR^{R_i^{O_2},R_j^{NO_3^-}}$ per amount of electron acceptor reacted (top part) and equivalence oxygen concentration $YR^{R_i^{O_2},R_j^{NO_3^-}}$ for a given nitrate concentration [NO_3^-] = 40 μ mol kg^{-1} (example value: as observed at the onset of nitrate consumption in Santa Monica Basin Hofmann et. al., 2013c). Both values are given for all combinations of an oxygen consuming reaction and a nitrate consuming reaction from Table 2.

$[\mathbf{O_2}]^{\mathbf{R_i^{O_2}, R_j^{NO_3^-}}}$	$R_1^{NO_3^-}$	$R_2^{NO_3^-}$	$R_3^{NO_3^-}$	$R_4^{NO_3^-}$	$R_5^{NO_3^-}$	$R_6^{NO_3^-}$	$R_7^{NO_3^-}$	$R_8^{NO_3^-}$
$R_1^{O_2}$	39.8	37.8	37.5	31.1	29.0	21.8	11.0	9.3
$R_2^{O_2}$	46.5	44.2	43.8	36.4	33.9	25.4	12.9	10.8
$\mathbf{CR^{R_i^{O_2}, R_j^{NO_3^-}}}$	$R_1^{NO_3^-}$	$R_2^{NO_3^-}$	$R_3^{NO_3^-}$	$R_4^{NO_3^-}$	$R_5^{NO_3^-}$	$R_6^{NO_3^-}$	$R_7^{NO_3^-}$	$R_8^{NO_3^-}$
$R_1^{O_2}$	1.00	1.06	1.07	1.28	1.38	1.84	3.63	4.31
$R_2^{O_2}$	0.86	0.91	0.91	1.10	1.18	1.57	3.11	3.69

Table 4: Diffusion limited free energy crossover oxygen concentration $[O_2]_{cr}^{R_i^{O_2}, R_j^{NO_3^-}}$ (upper panel) and the respective concentration crossover ratio $CR^{R_i^{O_2}, R_j^{NO_3^-}}$ (lower panel) for a given nitrate concentration $[NO_3^-]$ = 40 μ mol kg^{-1} (example value: as observed at the onset of nitrate consumption in Santa Monica Basin (Hofmann et. al., 2013c). Both values are given for all combinations of an oxygen consuming reaction and a nitrate consuming reaction from Table 2.

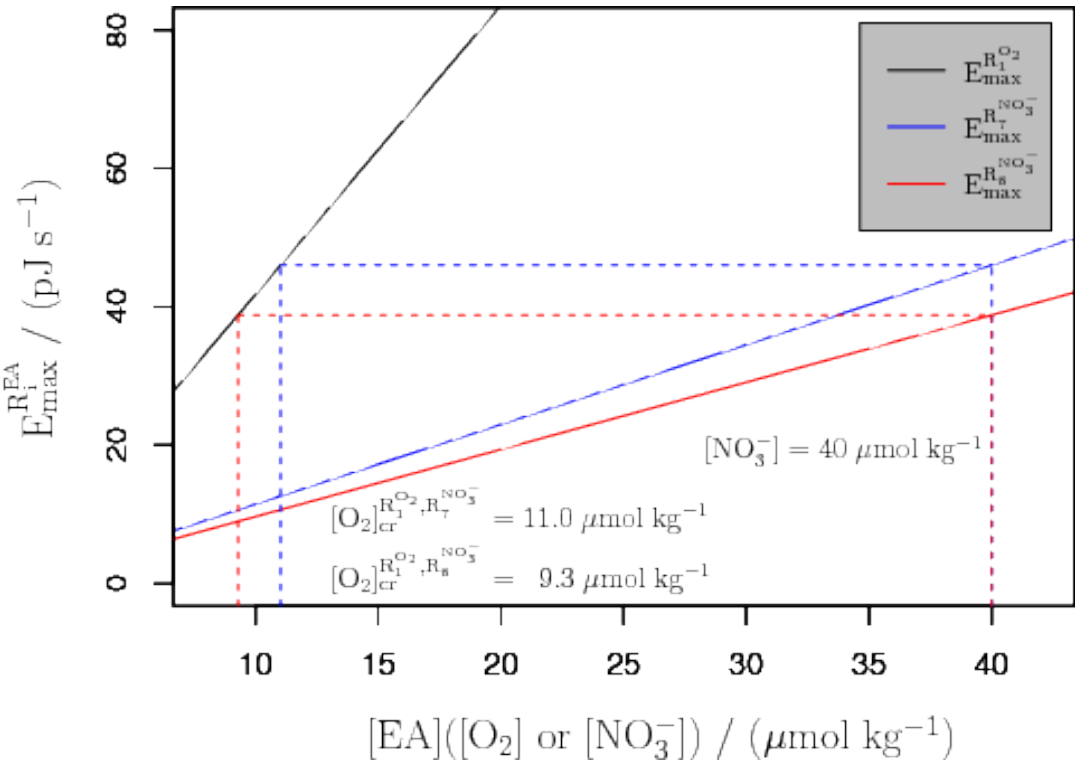

Figure 1: Graphically determining $[O_2]_{cr}^{R_i^{O_2},R_j^{NO_3^-}}$. Consider the reaction pairs $(R_1^{O_2}, R_8^{NO_3^-})$ and $(R_1^{O_2}, R_7^{NO_3^-})$ (see Table 2 for reactions): $E_{max}^{R_i^{EA}}$ for both reactions can be plotted in the same graph. Drawing a vertical line at the given value for $[NO_3^-]$ (here without loss of generality 40 μ mol kg $^{-1}$) and intersecting the $E_{max}^{R_7^{NO_3^-}}$ line (blue) gives $E_{max}^{R_7^{NO_3^-}}$ for $[NO_3^-]$ = 40 μ mol kg $^{-1}$. Extending a line horizontally from this point to the $E_{max}^{R_1^{O_2}}$ line and determining the abscissa position of the intersection provides the oxygen concentration where $E_{max}^{R_1^{O_2}}([O_2]) = E_{max}^{R_7^{NO_3^-}}([NO_3^-])$, which is by definition $[O_2]_{cr}^{R_1^{O_2},R_7^{NO_3^-}}$ and has a value of $\approx$ 11.0 μ mol kg $^{-1}$ for the given example. $[O_2]_{cr}^{R_1^{O_2},R_8^{NO_3^-}}$ can be determined equivalently (red lines).

609

610

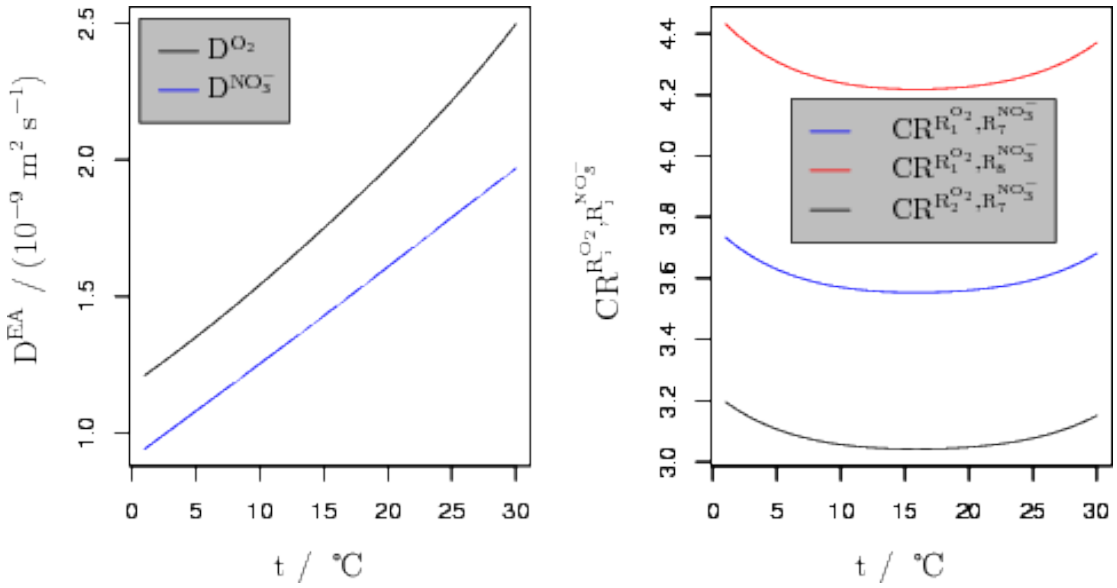

611

612 **Fig. 2:** **Left panel.** Temperature dependency of the molecular diffusion coefficients for oxygen
613 (D^{O_2}) and for nitrate ($D^{NO_3^-}$) (Boudreau, 1996).

614 **Right panel.** Temperature dependency of $CR^{R_i^{O_2},R_j^{NO_3^-}}$ for three different reaction combinations
615 and $[NO_3^-] = 40\ \mu$ mol kg $^{-1}$.
616

617

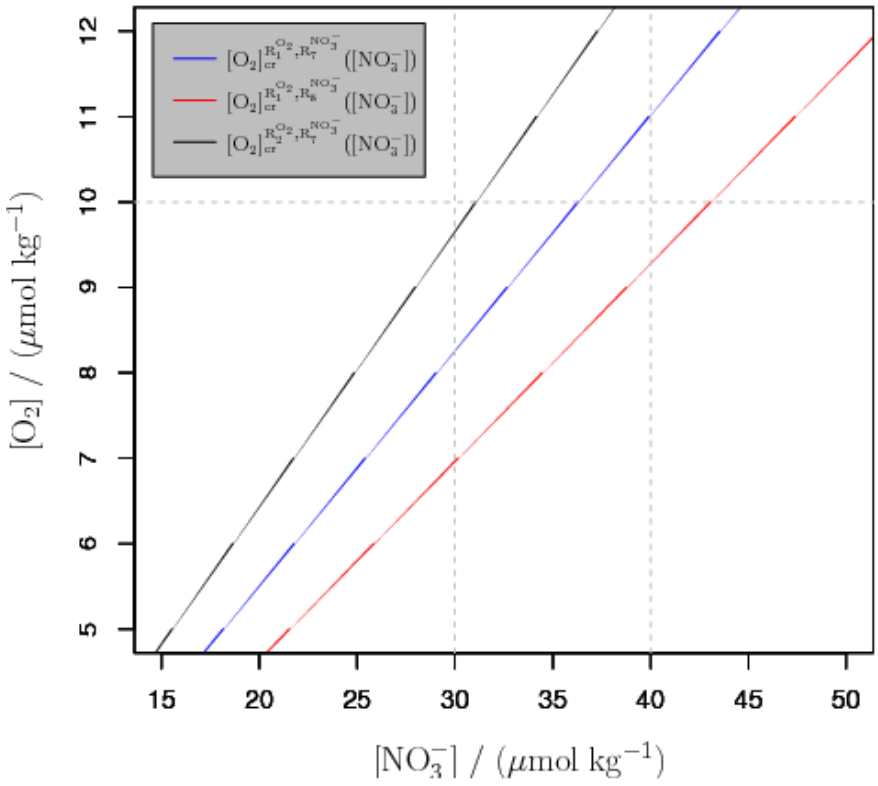

Fig. 3: Nitrate concentration [NO $_3^-$] versus the oxygen energy and diffusive limitation crossover concentration $[O_2]_{cr}^{R_i^{O_2},R_j^{NO_3^-}}$ calculated as a function of [NO $_3^-$] for three different oxygen and nitrate reaction combinations (solid lines). The gray, dashed vertical lines represent two typical ambient nitrate concentrations around the onset of nitrate consumtion: 30 μ kg $^{-1}$: approximate nitrate concentration at the onset of NO $_3^-$ consumption at the VERTEX stations in the eastern tropical North Pacific (Rue et al.,1997); 40 μ: approximate nitrate concentration at the inflection point of the [NO $_3^-$] curve, i.e. the potential onset of NO_3 consumption off Santa Monica (Hofmann et. al., 2013 and Fig. 4). The gray, dashed, horizontal line represents the classical "suboxia" threshold (e.g. Shaffer 2009).

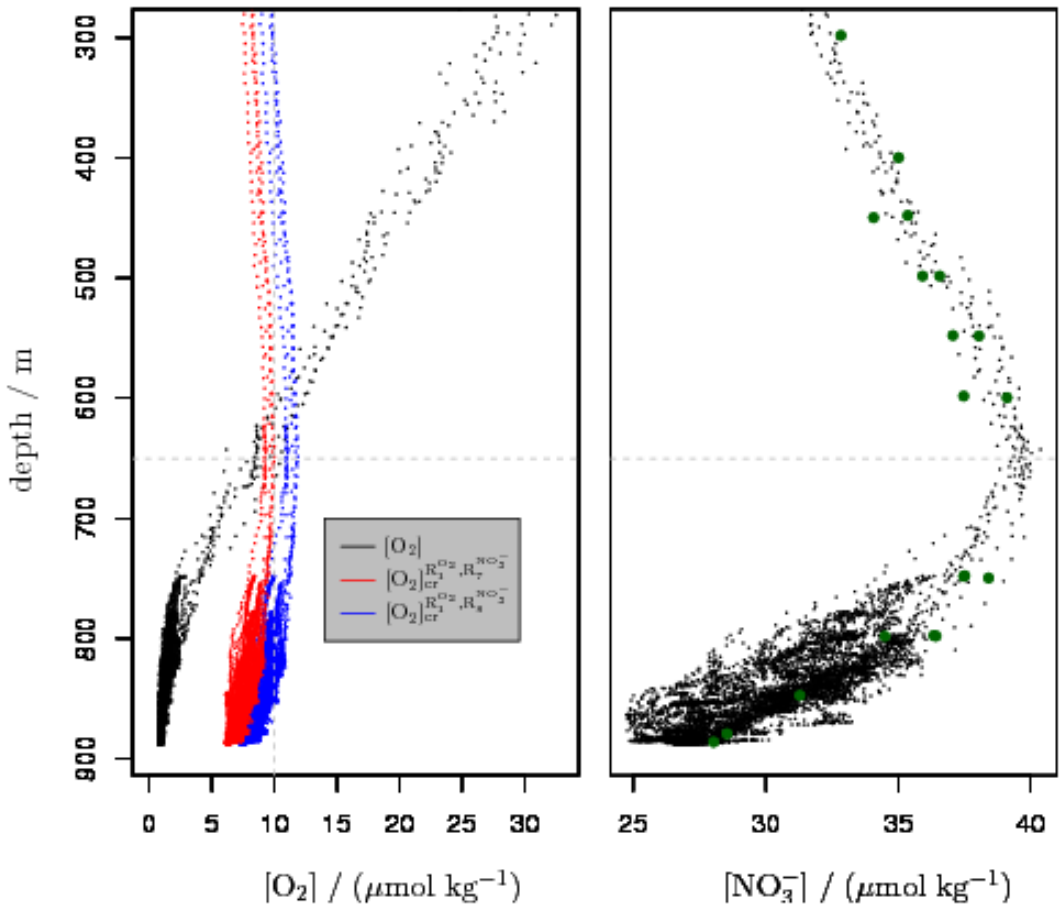

Figure 4: [O $_2$], [NO $_3^-$], $[O_2]_{cr}^{R_1^{O_2},R_7^{NO_3^-}}$, and $[O_2]_{cr}^{R_1^{O_2},R_8^{NO_3^-}}$ for depth profiles in the Santa Monica Basin, obtained by an AUV survey in June 2011 (Hofmann et. al., 2013). Large green dots in the right hand panel are laboratory determined nitrate values from water samples obtained with an AUV-board water sampling system. The horizontal, gray, dashed line at 650 m marks the inflection depth of the [NO $_3^-$] profile.

Appendix

5 Supplementary Material

$\mathbf{R_2^{O_2}}$	$106\,\overset{0}{C}H_2O \rightarrow 106\,\overset{+4}{C}O_2 + 106H_2O + 424e^-$ $16\overset{-3}{N}H_3 \rightarrow 16\overset{+5}{H}NO_3 + 128e^-$
$\cdot\ 138\vert$	$\overset{0}{O}_2 + 4e^- \rightarrow CO_2$
	$(CH_2O)_{106}(NH_3)_{16} + 138O_2 \rightarrow 106CO_2 + 16HNO_3 + 122H_2O$
$\mathbf{R_1^{O_2}}$	$(\overset{0}{C}H_2O)_{106}(NH_3)_{16} \rightarrow 106\overset{+4}{C}O_2 + 16NH_3 + 106H_2O + 424e^-$
$\cdot\ 106\vert$	$\overset{0}{O}_2 + 4e^- \rightarrow CO_2$
	$(CH_2O)_{106}(NH_3)_{16} + 106O_2 \rightarrow 106CO_2 + 16NH_3 + 106H_2O$
$\mathbf{R_2^{NO_3^-}}$	$(\overset{0}{C}H_2O)_{106}(NH_3)_{16} \rightarrow 106\overset{+4}{C}O_2 + 16NH_3 + 106H_22O + 424e^-$
$\cdot\ 84.8\vert$	$\overset{+5}{H}NO_3 + 5e^- \rightarrow \frac{1}{2}\overset{0}{N}_2 + \ldots$
	$(CH_2O)_{106}(NH_3)_{16} + 84.8HNO_3 \rightarrow 106CO_2 + 16NH_3 + 42.4N_2 + 148.4H_2O$
$\mathbf{R_3^{NO_3^-}}$	$106\overset{0}{C}H_2O \rightarrow 106\overset{+4}{C}O_2 + 106H_2O + 424e^-$ $16\overset{-3}{N}H_3 \rightarrow 8\overset{0}{N}_2 + 48e^-$
$\cdot\ 94.4\vert$	$\overset{+5}{H}NO_3 + 5e^- \rightarrow \frac{1}{2}\overset{0}{N}_2 + \ldots$
	$(CH_2O)_{106}(NH_3)_{16} + 94.4HNO_3 \rightarrow 106CO_2 + 55.2N_2 + 177.2H_2O$
$\mathbf{R_1^{NO_3^-}}$	$106\overset{0}{C}H_2O \rightarrow 106\overset{+4}{C}O_2 + 424 + \ldots$
$\cdot\ 53\vert$	$\overset{+5}{H}NO_3 + 8e^- \rightarrow \overset{-3}{N}H_3 + \ldots$
	$(CH_2O)_{106}(NH_3)_{16} + 53HNO_3 \rightarrow 106CO2 + 69NH_3 + 53H_2O$
$\mathbf{R_7^{NO_3^-}}$	$106\overset{0}{C}H_2O \rightarrow 106\overset{+4}{C}O_2 + 106H_2O + 424e^-$
$\cdot\ 212\vert$	$\overset{+5}{H}NO_3 + 2e^- \rightarrow \overset{+3}{H}NO_2 + \ldots$
	$(CH_2O)_{106}(NH_3)_{16} + 212HNO_3 \rightarrow 106CO_2 + 212HNO_2 + 16NH_3 + 106H_2O$
$\mathbf{R_8^{NO_3^-}}$	$106\overset{0}{C}H_2O \rightarrow 106\overset{+4}{C}O_2 + 106H_2O + 424e^-$ $16\overset{-3}{N}H3 \rightarrow 16\overset{+3}{H}NO_2 + 96e^-$
$\cdot\ 260\vert$	$\overset{+5}{H}NO_3 + 2e^- \rightarrow \overset{+3}{H}NO_2 + \ldots$
	$(CH_2O)_{106}(NH_3)_{16} + 260HNO_3 \rightarrow 106CO_2 + 276HNO_2 + 122H_2O$

Table A.1: Explicit redox balances for representative organic matter oxidation reactions (Tab. 1).

name	**formula**	$\mathbf{\Delta Gf^0}$	comment
α-D-glucose	$C_6H_{12}O_6$	-917.220	
oxygen	O_2	0.000	
carbon dioxide	CO_2	-394.359	
water	H_2O	-237.178	
nitrate	NO_3^-	-111.340	
nitrite	NO_2^-	-37.200	
nitric acid	HNO_3	-151.210	$H + NO_3^-$
nitrous acid	HNO_2	-77.07	$H + NO_2^-$
ammonium	NH_4^+	-79.370	
ammonia	NH_3	-26.570	
proton	H^+	-39.870	pH=7
nitrogen gas	N_2	0.000	
elemental sulfur	S^0	0.000	
hydrogen sulfide	H_2S	-33.560	
sulfate	SO_4^{2-}	-744.630	

Table A.2 Energies of formation of relevant chemical species. Excerpt from table 15 of Thauer et al.(1977), values in $\frac{\text{kJ}}{\text{mol}}$, at standard conditions (unit activities: 1 $\frac{\text{mol}}{\text{kg}}$; pH=7 (thus changing $[H^+]$ from unit concentration); T=25 °C).

$\mathbf{R_2^{O_2}}$ $138\vert$	$(CH_2O)_{106}(NH_3)_{16} + 138O_2 -> 106CO_2 + 16HNO_3 + 122H_2O$
	$\frac{1}{138}((CH_2O)_{106}(NH_3)_{16}) + O_2 -> \frac{53}{69}CO_2 + \frac{8}{69}HNO_3 + \frac{61}{69}H_2O$
$\mathbf{R_1^{O_2}}$ $/106\vert$	$(CH_2O)_{106}(NH_3)_{16} + 106O_2 -> 106CO_2 + 16NH_3 + 106H_2O$
	$\frac{1}{106}((CH_2O)_{106}(NH_3)_{16}) + O_2 -> CO_2 + \frac{16}{106}NH_3 + H_2O$
$\mathbf{R_2^{NO_3^-}} \cdot \frac{5}{424}\vert$	$(CH_2O)_{106}(NH_3)_{16} + 84.8HNO_3 -> 106CO_2 + 16NH_3 + 42.4N_2 + 148.4H_2O$
	$\frac{5}{424}((CH_2O)_{106}(NH_3)_{16}) + HNO_3 -> \frac{5}{4}CO_2 + \frac{10}{53}NH_3 + \frac{1}{2}N_2 + \frac{7}{4}H_2O$
$\mathbf{R_3^{NO_3^-}} \cdot \frac{5}{472}\vert$	$(CH_2O)_{106}(NH_3)_{16} + \frac{472}{5}HNO_3 -> 106CO_3 + \frac{552}{10}N_2 + \frac{886}{5}H_2O$
	$\frac{5}{472}((CH_2O)_{106}(NH_3)_{16}) + HNO_3 -> \frac{265}{236}CO_2 + \frac{69}{118}N_2 + \frac{443}{236}H_2O$
$\mathbf{R_5^{NO_3^-}}$ $/3\vert$	$7H_2O + 3NO_3 - + 4S^0 -> 3NH_4^+ + 4SO_4^{2-} + 2H^+$
	$\frac{7}{3}H_2O + NO_3 - + \frac{4}{3}S^0 -> NH_4^+ + \frac{4}{3}SO_4^{2-} + \frac{2}{3}H^+$
$\mathbf{R_1^{NO_3^-}}$ $/53\vert$	$(CH_2O)_{106}(NH_3)_{16} + 53HNO_3 -> 106CO_2 + 69NH_3 + 53H_2O$
	$\frac{1}{53}((CH_2O)_{106}(NH_3)_{16}) + HNO_3 -> 2CO_2 + \frac{69}{53}NH_3 + H_2O$
$\mathbf{R_7^{NO_3^-}}$ $212\vert$	$(CH_2O)_{106}(NH_3)_{16} + 212HNO_3 -> 106CO_2 + 212HNO_2 + 16NH_3 + 106H_2O$
	$\frac{1}{212}((CH_2O)_{106}(NH_3)_{16}) + HNO_3 -> \frac{1}{2}CO_2 + HNO_2 + \frac{4}{53}NH_3 + \frac{1}{2}H_2O$
$\mathbf{R_8^{NO_3^-}}$ $/260\vert$	$(CH_2O)_{106}(NH_3)_{16} + 260HNO_3 -> 106CO_2 + 276HNO_2 + 122H_2O$
	$\frac{1}{260}((CH_2O)_{106}(NH_3)_{16}) + HNO_3 -> \frac{53}{130}CO_2 + \frac{69}{65}HNO_2 + \frac{61}{130}H_2O$

Table A.3: Reformulation of representative organic matter oxidation reactions (Tab. 1) and dissimilatory nitrate reduction coupled to hydrogen sulfide oxidation (Sayama et al., 2005) standardized to electron acceptors.